

Calculating the energy profile of an enzymatic reaction on a quantum computer.

Patrick Ettenhuber^{†,*}, Mads Bøttger Hansen[†], Irfansha Shaik^{A,†}, Stig Elkjær Rasmussen^{†,‡}, Pier Paolo Poier[†], Niels Kristian Madsen[†], Marco Majland^{†,‡,§}, Frank Jensen^{§,†}, Lars Olsen^{||}, and Nikolaj Thomas Zinner^{†,‡}

*corresponding authors: Patrick Ettenhuber (pe@kvantify.dk)

[†]Kvantify Aps, DK-2100 Copenhagen, Denmark

[‡]Department of Physics and Astronomy, Aarhus University, DK-8000 Aarhus C, Denmark

[§]Department of Chemistry, Aarhus University, DK-8000 Aarhus C, Denmark

^ADepartment of Computer Science, Aarhus University, DK-8000 Aarhus C, Denmark

^{||}Novonosis A/S, DK-2800 Kgs. Lyngby, Denmark

ABSTRACT

Quantum computing (QC) provides a promising avenue toward enabling quantum chemistry calculations, which are classically impossible due to a computational complexity that increases exponentially with system size. As fully fault-tolerant algorithms and hardware, for which an exponential speedup is predicted, are currently out of reach, recent research efforts are dedicated to developing and scaling algorithms for Noisy Intermediate-Scale Quantum (NISQ) devices to showcase the practical utility of such machines. To demonstrate the utility of NISQ devices in the field of chemistry, we apply our recently developed FAST-VQE algorithm and a novel quantum gate reduction strategy based on propositional satisfiability together with standard optimization tools for the simulation of the rate-determining proton transfer step for CO₂ hydration catalysed by carbonic anhydrase resulting in the first application of a quantum computing device for the simulation of an enzymatic reaction. To this end, we have combined classical force field simulations with quantum mechanical methods on classical and quantum computers in a hybrid calculation approach. The presented technique significantly enhances the accuracy and capabilities of QC-based molecular modeling and finally pushes it into compelling and realistic applications. The framework is general and can be applied beyond the case of computational enzymology.

1 Introduction

Enzymes are remarkable biological molecules that act as catalysts. They can speed up chemical reactions, often by many orders of magnitude, under the moderate conditions that living organisms thrive in. At the same time, enzymes can be exceptionally selective towards target substrates, making chemical reactions extremely fast while reducing undesirable side reactions.

These striking catalytic properties are the result of natural evolution that has slowly optimized and shaped enzymes as we know them today. Understanding the underlying catalytic mechanism is not only interesting in its own right, but it also holds immense potential to improve our quality of life. For example, this knowledge can pave the way for developing novel life-saving drugs, cleaner bioremediation procedures, and more sustainable chemical processes. In medicinal chemistry, for example, the inhibition of enzymes via selective inhibitors can have many therapeutic applications, a prime example is antibiotics that kill harmful bacteria in a human host by selectively blocking enzymes in central bacterial metabolic pathways. From an industrial point of view, the replacement of traditional catalysts with enzymes could make large-scale processes more sustainable by reducing operating temperatures and pressures and by replacing organic solvents with water. Thus, considerable effort has been spent elucidating the underlying principles of enzymatic catalysis, both experimentally and computationally. In fact, computational enzymology has become an important tool that complements experimental studies of mechanisms and it can be divided into different topics, each characterized by dedicated computational approaches.

The large number of calculations involved in ligand screening for drug discovery often demands the use of parameterized energy functions which are computationally cheap but not suitable for calculating chemical properties. Such parametrized energy functions are typically not applicable for calculating kinetic constants derived from energy barriers, as encountered in enzymatic catalysis. For this purpose, quantum mechanical methodologies are required and it is generally attempted to obtain chemical accuracy, defined as 1 kcal/mol, for quantitative predictions. Kohn-Sham Density Functional Theory (DFT) is the most widely used electronic structure method in computational chemistry as it introduces electronic correlation at a moderate computational cost. While in principle mathematically exact, the true form of the exchange-correlation functional is unknown

and thus it is, in practice, often impossible to reach chemical accuracy with DFT. Furthermore, the lack of a clear indicator for reliable results can make it difficult to assess the actual accuracy of DFT results, diminishing its value as a predictive tool. Wave function-based correlated methods, on the other hand, offer the potential for exact solutions¹. However, this comes at a significant computational cost making it only practical for small molecules.

Despite tremendous progress wave function-based methods and DFT are not applicable for full proteins. Catalytic mechanisms, however, usually occur in small regions of enzymes, making it thus possible to separate the systems into regions of low and high accuracy. These multi-scale modelling methods have already been developed in the '70s by Levitt and Warshel²⁻⁴. Wave function methods or, more often, DFT may be used for the high-accuracy calculations, but since these multiscale methods require rather large high-accuracy regions the disadvantages of DFT and wave function-based methods still apply and therefore novel approaches are desired.

As envisioned by Richard Feynman quantum computing promises to simulate quantum systems efficiently. The high complexity and steep scaling associated with the simulation of quantum systems on classical hardware could be alleviated with fault-tolerant quantum hardware. This could lead to a dramatic impact on the modelling accuracy for large molecules. It is reasonable to expect that the same systems modelled at present with Kohn-Sham DFT on classical devices will, in a not-too-distant future, be treated with highly-accurate wave function methodologies on quantum computers. This optimistic outlook is fueled by the ongoing advancements in quantum hardware technology and the development of powerful quantum algorithms.^{5,6} Despite this enormous progress, current Noisy Intermediate-Scale Quantum (NISQ) devices are not yet fault-tolerant, and thus only capable of executing simple computational circuits. The frequent errors on such machines will render the output useless if the algorithms are too complicated. Thus a range of algorithms has been developed specifically for these devices⁵. Recently, the question was raised whether NISQ devices were able to perform useful work without the expectation of any speedup compared to classical devices⁷, coining the expression *quantum utility*. We have attempted to use a NISQ device for the task of describing the energy along the reaction coordinate of an enzymatic reaction and with a clear path towards the realm where it becomes hard to verify the results on a classical computer, as recently reported in a study by IBM⁸.

To achieve this, we have developed and applied a fully-automated hybrid multi-level quantum computing strategy capable of modelling enzymatic reactions. This work focuses on modelling carbonic anhydrase (CA), an enzyme ubiquitous in nature and first discovered in 1932 for its role in regulating the blood pH by catalyzing the hydration of carbon dioxide with the resulting release of carbonic acid⁹. More recently, CA has attracted attention globally as it offers the potential to address challenges associated with climate change, specifically when reducing the atmospheric CO₂ concentration.

In particular, we have studied the energy profile of the rate-determining step of the reaction consisting of the proton transfer between a water molecule and Histidine 64 (H64), mediated by three additional solvent molecules as well as by a coordinated zinc atom^{10,11}. The full catalytic cycle for CA is schematically shown in Figure 1.

A correlated wave-function method is dedicated to a part of the active site where the atoms are directly involved in the bond breaking/formation. The correlated wave function is optimized via the efficient Fermionic Adaptive Sampling Theory VQE (FAST-VQE) algorithm¹² on the IonQ Aria trapped ion quantum device. This accurately modelled portion of the system is embedded in a Kohn-Sham DFT electron density calculation in a defined QM region. The remaining system is treated classically with the Geometry, Frequency, Noncovalent-Force Field (GFN-FF)^{13,14} method and using an ONIOM description¹⁵. This is thus the first application of quantum hardware for describing an enzymatic reaction using a multi-scale embedding framework. There have been examples on hardware where less of the environment has been captured¹⁶ and where the multi-scale framework has not been used in a quantum hardware setting¹⁷⁻¹⁹. The presented framework is general and can be applied beyond biologically relevant systems, pushing quantum computing-aided molecular modelling into the realm of realistic applications.

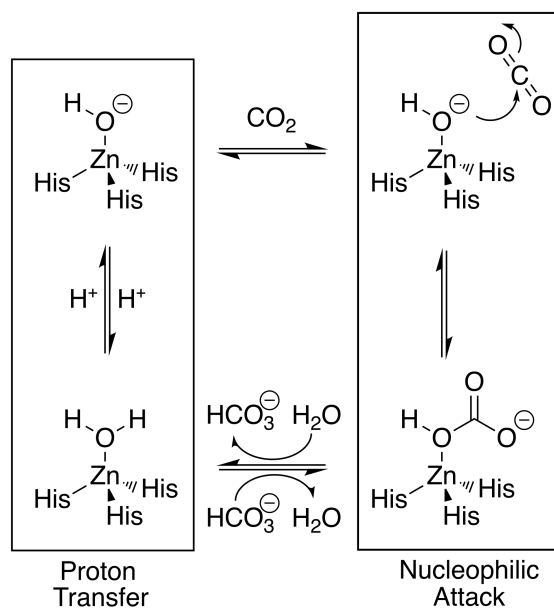


Figure 1. Catalytic cycle for the hydration of CO_2 in carbonic anhydrase enzymes with emphasis on the zinc ion. On the left, it is shown the proton transfer (rate-determining) step investigated in this work while the nucleophilic attack step is represented on the right.

2 Results

Simulating the energy profile of an enzymatic reaction on a quantum computer is a complex task that necessitates a multifaceted approach. This involves several key steps: preparing the enzymatic system, identifying and optimizing the reaction coordinate, strategically dividing the molecule using a quantum mechanics/molecular mechanics (QM/MM) approach, and finally coupling the classical and quantum calculations within the quantum region. In the next section, we will elaborate on all of these steps.

2.1 System and reaction coordinate preparation

The enzyme structure used in this work refers to the Human Carbonic Anhydrase II (PDB-ID 2CBA), Figure 2, as prepared and provided in the supplementary material of Fu *et al.*²⁰. The reaction coordinate was identified using our implementation of the nudged elastic band (NEB) method²¹ while modelling the structures with the ONIOM method, using GFN-FF²² method as the low-level method and the Geometry, Frequency, Noncovalent, extended Tight Binding v2 (GFN2-xTB)²³ method as the high-level method. Both these methods were used through the xtb¹⁴ program package.

To construct the initial path for the NEB calculation, suitable reactant and product structures first had to be obtained. Our reactant structure was found by optimizing the geometry of the reactant structure from Fu *et al.*²⁰ using our chosen ONIOM[GFN2-xTB:GFN-FF] model (with implicit water, using the analytical linearized Poisson–Boltzmann (ALPB) model²⁴). The geometry-optimization was converged to a maximum atomic gradient component of 10^{-3} a.u. $\approx 1.2 \text{ kcal mol}^{-1} \text{ \AA}^{-1}$. The product structure corresponding to the equivalent overall protein conformation was determined by manually moving only the hydrogen atoms involved in the proton transfer, to form a structure with the proper product topology; this structure was then similarly geometry optimized, and the initial path for the NEB calculation was obtained by linearly interpolating atomic positions between these reactant/product structures.

By constructing the NEB input in this way, we achieved minimal motion of the remote chemical groups of the enzyme, ensuring that there were only contributions to energy changes along the reaction path, that stemmed from conformational rearrangements associated with the proton transfer reaction. In a typical molecular dynamics simulation, this problem would be handled by adequately sampling the conformational space, which is prohibitive on a quantum computer due to the vast amount of single-point energy evaluations required. Instead, we have chosen a sample-free approach resulting in reaction enthalpies rather than free energies. This effective freezing of the rest of the protein is necessary for the correct interpretation of the energy path. It should be noted that any tunnelling effects in the proton transfer reaction are neglected in this study.

The NEB path optimization was also converged to a maximum atomic gradient component of 10^{-3} a.u. $\approx 1.2 \text{ kcal mol}^{-1} \text{ \AA}^{-1}$. The resulting 10 points provide the input structures for the accurate correlated wave function calculations performed on quantum

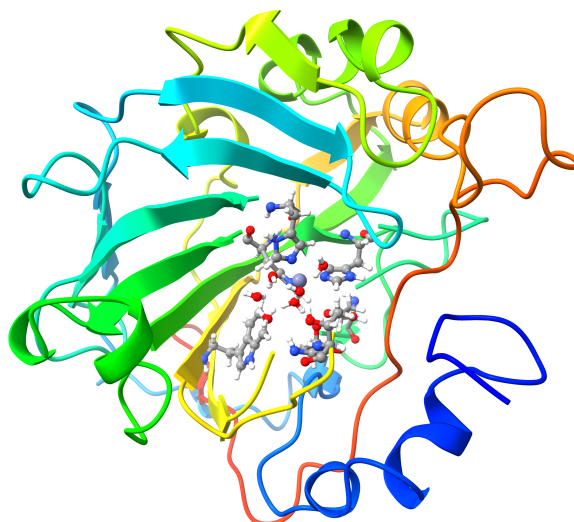


Figure 2. Representation of the Human Carbonic Anhydrase II (PDB-ID 2CBA). Explicit solvent molecules have been removed except those close to the active site. The portion of the enzyme-treated quantum mechanically is shown with a ball-and-stick representation while the rainbow ribbon representation indicates the remaining portion of the system.

hardware with the multi-layer embedding strategy described below. The full enzyme structures along the reaction coordinate can be found in the supporting information material.

2.2 Multi-layer embedding

The present section describes the fully automated multi-layer embedding framework as implemented in our software suite. Besides hyper-parameter settings like the cutoff radius for the quantum mechanics (QM) region and certain algorithmic choices, no additional user-input is required.

Multiple layers of embedding were used for the quantum calculation while adequately treating the environment. The outermost layer of the protein is coupled to the external environment by the ALPB continuum model for water implemented in the extended tight-binding (xTB)^{14,22,24} package. The outermost portion of the protein itself is described by molecular mechanics (MM) with the GFN-FF force field. This classically described region is coupled to a region about 4.8 Å in radius around the active site. The active site is described by QM by embedding a FAST-VQE wave function into the region described by DFT. The driver for the QM calculations on classical hardware is PySCF²⁵⁻²⁷ while the implementation of the energy component evaluated on a quantum computer is discussed profusely later in this section.

Since we use an ONIOM¹⁵ description of the system, we may write the total energy as

$$E_{\text{tot}} = E_{\text{full}}^{\text{MM}} - E_{\text{region}}^{\text{MM}} + E_{\text{region}}^{\text{QM}}, \quad (1)$$

where the obvious approximations commonly encountered in molecular modelling may be summarized as

1. The continuum water model is only accounted for in $E_{\text{full}}^{\text{MM}}$ and neglected in the inner region calculations as the water molecules around the active site have been modelled explicitly.
2. When partitioning the system, hydrogen caps are introduced in the region on the boundaries between the MM and QM regions as typically done in QM/MM methods.

For the QM calculations around the active site, we include all residues and molecules that have at least one atom within a 4.8 Å radius around the active site (or more specifically, around the focus water oxygen atom and the two hydrogens involved in the proton transfer reaction) up to the first alpha carbon atoms outside of this radius. This applies for side chains and backbone portions. Non-peptide groups and molecules are included entirely. The connections of these alpha carbons are then cut and capped with hydrogen atoms following a standard procedure in QM/MM embedding calculations. The QM region is determined once for the transition state structure and reused in the remaining calculations along the reaction coordinate to ensure consistent results.

An accurate description of the QM region is particularly important as this region includes the most chemically relevant portion of the system taking part in the proton transfer reaction under consideration. We choose the wave function in DFT projective embedding (wf@DFT) scheme²⁸ as the method for modelling the QM region due to its simple structure. In particular, the method combines correlated wave function methodologies with DFT, thus inheriting the high accuracy of the former while preserving a tractable computational cost necessary to model larger and more realistic molecular systems. Other analogous techniques could also be employed^{17,29,30}, however, in connection with quantum computing applications, the chosen wf@DFT approach provides notable advantages as it only relies on the energy of the correlated portion of the QM region and is conceptually simple, although other algorithms are available³¹. Here, we use the measurement-efficient FAST-VQE quantum algorithm¹² for the correlated region. Note that the wf@DFT method has recently been used on a NISQ device in combination with the Adaptive Derivative-Assembled Pseudo-Trotter Ansatz Variational Quantum Eigensolver (ADAPT-VQE) method³² for modelling the potential energy surface of the nitrile group dissociation reaction in butyronitrile¹⁶.

The wf@DFT embedding method has been described in detail before^{16,28} and thus we will focus on the parts that determine the accuracy of the overall calculation. Using this method, the QM energy $E_{\text{region}}^{\text{QM}}$ of the total QM/MM embedding scheme from Eq. (1) may be written as

$$E_{\text{region}}^{\text{QM}} = E_{\text{EMB}}[\Psi_A] + E_{\text{DFT}}[\mathbf{D}_A + \mathbf{D}_B] - E_{\text{DFT}}[\mathbf{D}_A], \quad (2)$$

where A denotes the orbital space of the high-accuracy calculation and B is the complement of A . E_{EMB} denotes the embedding energy of the high-accuracy calculation resulting in a wave function for atomic region A and may be obtained from any correlated wave function. We use the FAST-VQE algorithm to provide this quantity.

To arrive at an effective embedding Hamiltonian that can be encoded and evaluated on a NISQ device, a couple of classical preparation steps are necessary, i.e. orbital localization, orbital assignment, and active space selection, which we will discuss in the following sections. We will conclude the discussion by briefly describing the FAST-VQE algorithm.

2.2.1 Orbital localization and assignment

To separate the energy in Eq. (2) consistently, each occupied molecular orbital must be assigned to one of the two subsystems A and B respectively. This is done by obtaining localized molecular orbitals through a suitable unitary transformation. Several standard algorithms for this task are available and we chose intrinsic bonding orbitals³³. Note that wf@DFT only requires localized occupied orbitals while there is no restriction on the form of the virtual orbitals. We will use this fact in the active space selection.

After the localization, the orbitals need to be assigned to atomic centers and several different choices are possible. We have chosen to use a simple scheme based on orbital expansion coefficients, see Appendix A.

2.2.2 Active space selection

The orbital subspace assigned to subsystem A is typically too large to encode the effective electronic Hamiltonian into a current NISQ device. To efficiently fit the problem size to the available hardware, it is thus necessary to construct a representation of the subspace Hamiltonian that captures the main physical effects of *all* points along the reaction coordinate. Therefore, we will use a frozen natural orbital (FNO) approach³⁴ based on MP2 amplitudes.

Choosing an active space starts with selecting the number of orbitals and the number of electrons. Since the number of orbitals in the active space sets requirements on the hardware, this number may be seen as a constant due to the limited hardware sizes available. The number of electrons is important for the accuracy of the final calculation. For the remainder of this article, we use an active space of 6 electrons in 6 spatial orbitals. Further details about the active space construction are given in Appendix B.

2.2.3 Subspace calculations

After defining the active space a subspace Hamiltonian is constructed and prepared for the correlated calculation using the Jordan-Wigner mapping³⁵. We then use the FAST-VQE algorithm¹² for all correlated electronic structure calculations on a quantum computer. Here we provide the necessary background that allows us to discuss the computational details.

In FAST-VQE, a wave function ansatz is built adaptively by adding parameterized operators from an operator pool \mathcal{A} to the ansatz in each iteration. The ansatz at the k th iteration of the algorithm may be written as

$$|\Psi_k\rangle = \prod_{i=k}^1 e^{\theta_i \hat{\kappa}_i} |\text{HF}\rangle, \quad (3)$$

where the excitation operator $\hat{\kappa}$ along with the tunable parameter θ are introduced at each iteration i and $|\text{HF}\rangle$ is the Hartree-Fock (HF) reference state. Using exact excitation operators would result in too deep circuits, thus we are using a corrected version of the qubit excitation-based³⁶ operators in the operator pool \mathcal{A} containing only one and two-body particle-hole excitations, see Appendix C.

This adaptive approach was originally introduced by the ADAPT-VQE algorithm³², yet there is a difference in how the operators are selected in the FAST-VQE algorithm. In ADAPT-VQE, the metric g_μ used to assign importance to an operator $\hat{\kappa}_\mu$ in the next $k + 1$ iteration relies on the energy gradient computed with respect to the associated operator parameter θ_μ , Eq. (4), thus requiring a complete measurement for each operator in the operator pool \mathcal{A} .

$$g_\mu = \left(\frac{\partial E^{(k+1)}}{\partial \theta_\mu} \right)_{\theta_\mu=0} = \langle \Psi^{(k+1)} | [\hat{H}, \hat{\kappa}_\mu] | \Psi^{(k+1)} \rangle. \quad (4)$$

Instead, in FAST-VQE, the importance of an operator for the next $k + 1$ iteration is weighted by the heuristic α_μ according to Eq. (5), where a multiset of Slater determinants \mathcal{S} is sampled from $|\Psi^{(k)}\rangle$ in the computational basis

$$\alpha_\mu = \sum_{D_i \in \mathcal{S}} \sum_{D_j \in \mathcal{S}} \langle D_i | \hat{\kappa}_\mu \hat{H} | D_j \rangle, \quad \forall \mu \in \mathcal{A}. \quad (5)$$

In contrast to measuring expectation values, sampling is rather efficient on a quantum device and Eq. (5) is then evaluated on a classical computer. This reduces the measurement overhead per iteration to just 1 compared to the at least $O(N^6)$ measurements (N being the number of orbitals in the system) required in the ADAPT-VQE method. This has proven to be a simple and robust procedure for constructing wave functions on a quantum computer.

Validation of FAST-VQE results is straightforward as we can use the subspace HF energy and leverage an additional subspace complete active space configuration interaction (CASCI) calculation. The former provides the starting point for FAST-VQE and the latter provides essentially exact solutions within this space, acting as benchmarks for FAST-VQE's performance. This approach is feasible because exact diagonalization with CASCI in these small active spaces is computationally tractable with classical computers.

2.3 Computational details

Fragment A, modelled via a correlated wave function, has been chosen to include the oxygen atom in the middle of the three water molecules in the proton transfer reaction and the two moving hydrogen atoms. This region has five local occupied orbitals assigned at the transition state geometry (point 5 on the PES) that serves as a reference. Using the procedure outlined in sections 2.2.1 and 2.2.2, five occupied orbitals are assigned to the fragment and an active space is calculated for each point. The QM region is shown in Fig.3a, while Fig.3b also shows the electron density of fragments A and B respectively.

As discussed, the correlated wave function is generated from a complete active space of 6 electrons in 6 orbitals, embedded into an electron density computed with the B3LYP functional while the basis-set employed is Jensen's pcseg-1.³⁷

All SCF parameters were precomputed on Amazon EC2 `c5.12xlarge` instances, with 48 Intel Xeon Platinum 8000 series processors and 96Gb memory, and stored into suitable files. These files were then used to restart the calculations using Amazon Braket Hybrid Jobs on IonQ's Aria 1 quantum device. Parameters were optimized using an embedded state vector simulator. Additionally, three single points (initial, transition state, and product structures) were computed on Rigetti's Aspen-M-3 superconducting quantum device allowing us to compare different quantum hardware technologies as discussed later in the manuscript. For all calculations, we chose to extend the ansatz in Eq. (3) with one operator in each iteration and all experiments were conducted using 1024 shots on Aria 1 and Aspen-M-3.

2.4 Circuit optimization

Naively constructing the quantum circuits from the parametrized ansatz typically leads to long circuits that may not be executable on the targeted quantum hardware. IonQ's Aria has a limit of 950 single qubit gates which we encountered beyond 40 iterations of FAST-VQE. To reduce overall error and tackle hardware limitations, we apply circuit optimization. In particular, we mainly focus on reducing two-qubit CNOT gates and one-qubit gate count. While global optimization is not practical for CNOT reduction, peephole techniques where slices of the circuits are optimized individually are promising. We applied a standard slice-and-optimize strategy for optimizing CNOT sub-circuits. While several CNOT synthesis techniques exist, we applied SAT-based synthesis for optimal CNOT circuits³⁸. For one-qubit gate reduction, we employ Clifford Simplification from TKET³⁹. Since the circuits for excitation operators mainly contain Clifford gates, ZX-calculus-based rewrite rules perform well.

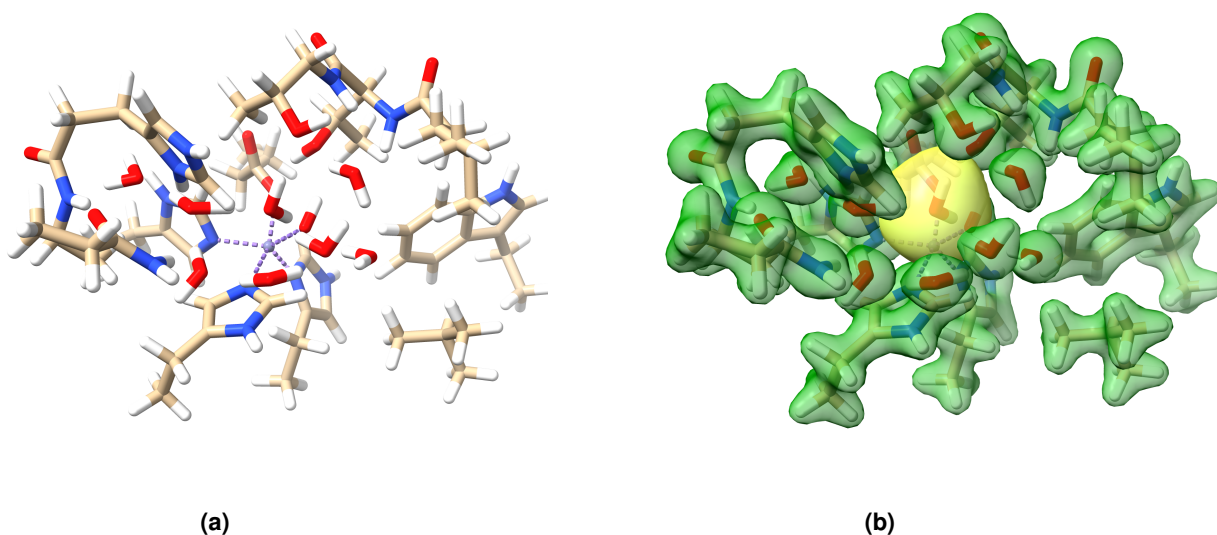


Figure 3. Subfigure (a) shows the portion of the enzyme defining the QM region and including the zinc atom, the key water molecules as well as the residues involved in the proton transfer process. Subfigure (b) includes the electron densities of both fragment A (light lime green) and fragment B (darker green) arising from the density matrices \mathbf{D}_A and \mathbf{D}_B of the system partitioned as described earlier.

2.5 Quantum experiments

The reaction coordinate identified as described in section 2.1 displays an energy barrier of circa 15.5 kcal/mol with respect to the initial reactants, in line with the barrier computed by Fu and coworkers, albeit their result refers to the free energy of the reaction and thus includes entropic contributions.²⁰ The resulting PES is shown in Fig.4. Note, that because the product region minimum is broad and shallow compared to the gradient convergence threshold of 10^{-3} a.u. ≈ 1.2 kcal mol⁻¹ Å⁻¹ the NEB calculation has found another product structure that is slightly lower in energy than the path endpoint.

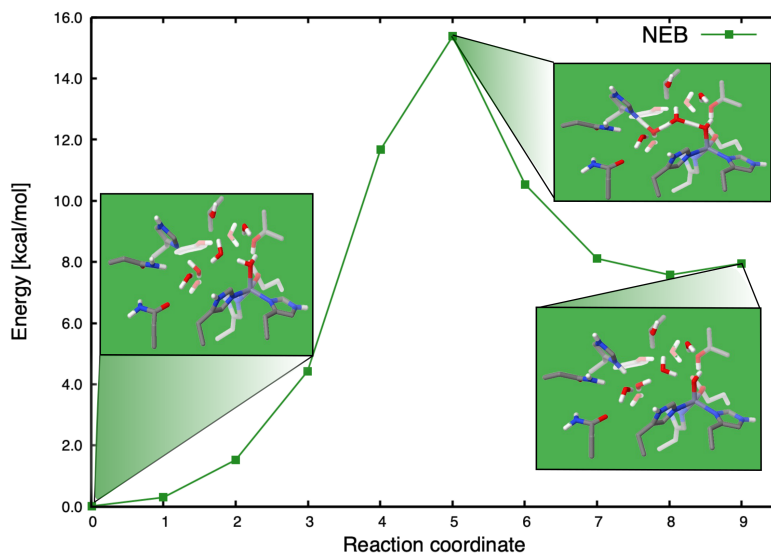


Figure 4. Potential energy surface obtained via a NEB calculation at the GFN2-xTB/GFN-FF level. The core portion of the initial, transition state and product structures used in the reaction path optimization are shown along the potential energy surface. The minimum at the end of the path is shallow and, with the convergence settings used, NEB was able to identify a point with a lower energy (point 8) than the optimized product structure (point 9).

The obtained reaction path provides the 10 input structures for the wf@DFT correlated calculations. Fig. 5 shows the PES obtained with the wf@DFT method on classical hardware providing the benchmark, called CAS(6,6), and the results obtained on the Aria-1 IonQ quantum system via the FAST-VQE algorithm with 40 iterations. Since the used methods are all variational,

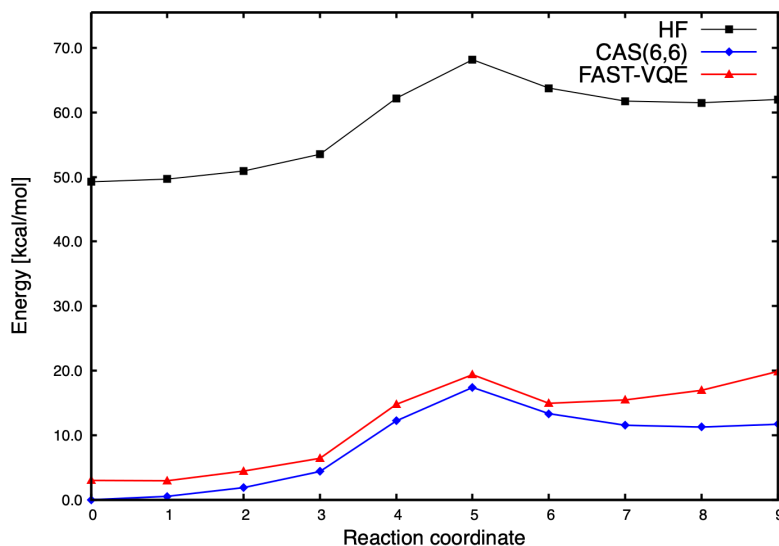


Figure 5. Potential energy surfaces obtained on classical hardware (black and blue) as well as on IonQ’s Aria-1 quantum hardware (red). The black (blue) curve refers to a HF (CASCI) treatment of the embedded subsystem A providing the starting point (exact reference) for a FAST-VQE calculation. The core portion of the initial, transition state and product structures used in the reaction path optimization are shown along the potential energy surface. All curves have been shifted such that the lowest energy point on the CAS(6,6) curve has zero energy.

the PES representing the classically exact CAS(6,6) benchmark (blue curve) is always below the FAST-VQE solution (red curve), which in turn is always below the HF solution (black curve), corresponding to ordering the methods by the number of free parameters. In general, the FAST-VQE solution is very close to the exact CAS(6,6) curve, although the last three points on the PES exhibit a larger error.

Albeit being efficient when building an ansatz adaptively, an increased number of FAST-VQE iterations comes with deeper circuits which may exceed the specific quantum hardware’s capabilities. For the Aria-1 quantum device, a maximum of 950 1 qubit gates are available, limiting the total number of FAST-VQE iterations to 40 with a standard gate compilation protocol. This impacts the overall accuracy of the calculation since it implies fewer free parameters to model the wave function. Convergence plots are displayed in Fig. 5 showing how the deviation from the classical solution evolves as a function of the iterations for three selected points including initial, transition, and final state structures along the PES. The convergence plots of the whole PES are given in the supplementary material.

To further push and probe convergence in terms of iterations, we selected a reactant, transition state, and product structures, structures 0,5 and 8, respectively, and ran the calculations with the FAST-VQE algorithm on Rigetti’s Aspen-M-3 system, powered by superconducting qubit-based quantum processors. There was no restriction on the number of gates and this device allowed us to reach 60 FAST-VQE iterations, exhibiting a continued consistent convergence towards the CAS(6,6) results in the additional 20 iterations, see Fig. 6. Despite the difference in the number of iterations, the convergence on IonQ’s Aria, and Rigetti’s Aspen-M-3 results show similar convergence patterns.

We note that, with 60 iterations it is possible to obtain errors very close or even below chemical accuracy (1 kcal/mol) along the whole reaction coordinate as exemplified in the three points above. This underlines how current advanced quantum hardware combined with state-of-the-art quantum algorithms such as the FAST-VQE approach can reach results inconceivable until recently in terms of accuracy and applicability.

Using the circuit optimization techniques described in section 2.4 it was possible to reach 55 FAST-VQE iterations due to a reduction of the ansatz circuits from 1016 to 660 single qubit gates and 540 to 533 two-qubit gates on IonQ’s Aria 1 system. The calculation exhibits the same convergence pattern as Rigetti’s Aspen-M-3 system for the last 15 iterations and thus reaches chemical accuracy for the transition state structure (structure 5), see the central plot in Fig. 6.

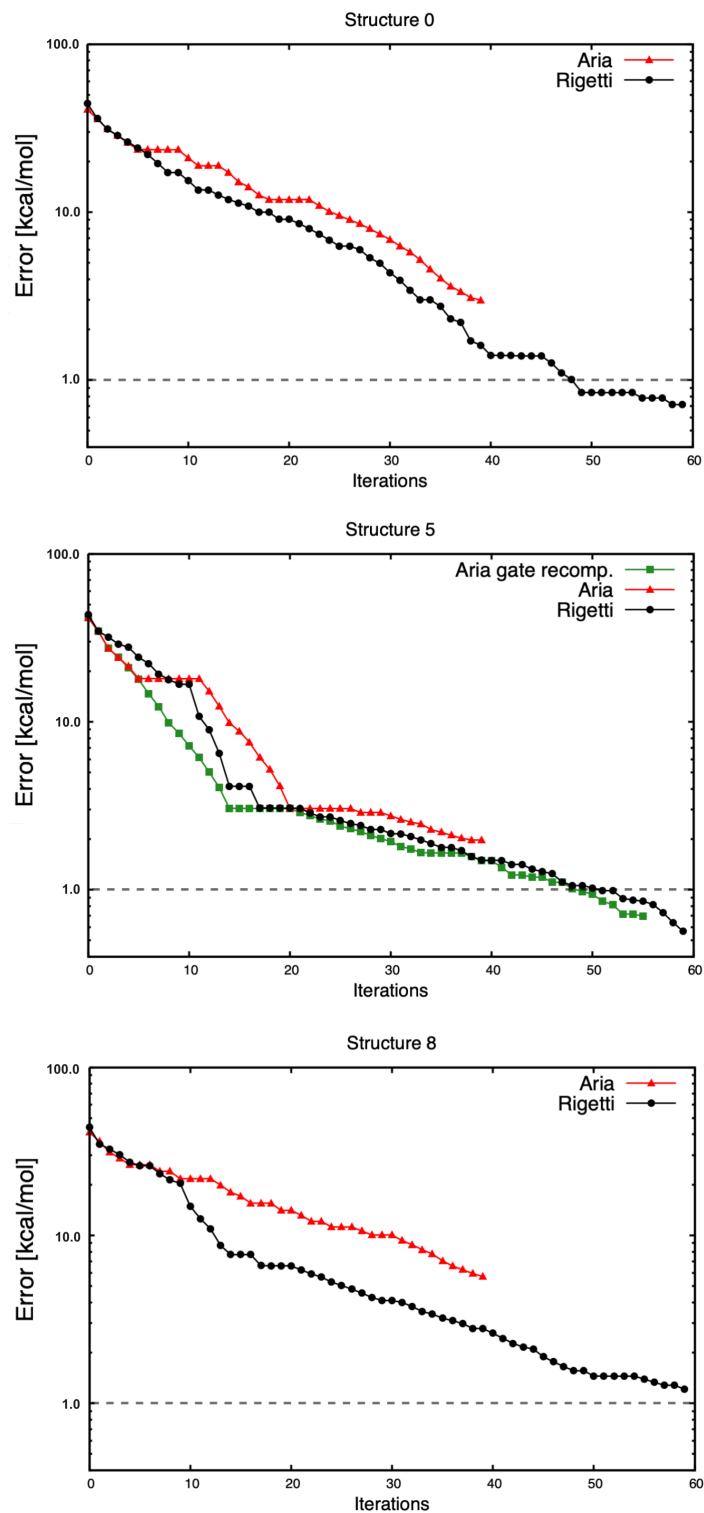


Figure 6. The subfigures show the error (in kcal/mol) between the FAST-VQE solution and the classical computing benchmark (CAS(6,6)) as a function of the number of iterations computed with IonQ and Rigetti quantum systems. The plots refer to structures 0, 5, and 8 along the proton transfer reaction coordinate. Chemical accuracy defined as 1 kcal/mol is highlighted in all plots by a dashed line. For structure 5, we additionally show the convergence pattern for Aria using the gate recompilation technique described in Section 2.4 up to 55 iterations.

3 Discussion

We have developed a fully automatic multi-scale quantum computational framework and applied it for the CO₂ hydration catalysed by Carbonic Anhydrase running on actual quantum hardware. To our knowledge, this is the first quantum computing application in modeling enzymatic reactions. The core region of the enzyme was treated quantum mechanically and partitioned into a higher accuracy part modelled with a correlated wave function optimized on quantum hardware via the efficient FAST-VQE algorithm. This accurate region was embedded into the remaining portion of the system modelled with DFT and the results show excellent agreement with classical computing benchmark calculations. In particular, we demonstrated chemical accuracy may be reached consistently even on today's error-prone quantum devices, provided that the depth of the quantum circuits can be kept below hardware-imposed limitations. Effective circuit optimization strategies help achieve shallower circuits. Eventually, more resilient or fault-tolerant architectures must take over to allow high-accuracy calculations when encountering complicated electronic structures. This problem is exacerbated when qubits are not all-to-all connected and more qubits are used necessitating additional operations and increasing the circuit depths. The remaining bottleneck in our framework is the parameter optimization via the variational quantum eigensolver (VQE) algorithm which is run using a state vector simulator due to its large measurement overhead. This hampers the scalability of the approach and although there exist techniques to avoid VQE^{8,40,41} this part remains a field of active research for demonstrating quantum utility.

The proposed framework presents the first scalable implementation for routinely running enzymatic catalysis applications on a quantum computer, while achieving chemical accuracy, despite the limitations of current quantum hardware. Due to a flexible implementation of the multilayer approach, it is possible to update the software as the hardware matures towards fault-tolerant machines enabling future-proof hybrid computing, e.g. by replacing FAST-VQE by a quantum phase estimation. Furthermore, the FAST-VQE algorithm itself may still be used in a fault-tolerant future as a state-preparation algorithm to improve the probability of success when running quantum phase estimation protocols.

The linear scaling with the system size promised by QC makes it possible to systematically approach the exact solution of electronic structure problems by using large active spaces. This will thus replace DFT when describing crucial portions of proteins or other chemical systems, finally surpassing DFT's transferability issues that hamper quantitative modelling of chemical reactions. On the other hand, for thermodynamic properties that require efficient sampling of the configuration space with millions or even billions of energy evaluations, it is difficult to foresee a path where the work is offloaded to a quantum computer. Even the best-case estimates for running quantum phase estimation on future quantum computers are about a day per energy evaluation⁴². Thus tremendous progress will be necessary to replace existing techniques, such as force-field-based molecular dynamics. Thus, quantum computing may be viewed as a tool that provides accuracy rather than speed in chemical calculations.

Nevertheless, quantum computing-based computational chemistry has a tremendous potential impact in accelerating enzyme development by complementing experimental approaches with highly predictive modeling, guiding the design and optimization of enzymes for various applications in biotechnology, medicine, and industry. Currently, activation energy calculations for enzymatic reactions are very time-consuming due to the size of the molecular system, and they may be imprecise since a multiconfigurational approach is out of reach. With the promise to tremendously speed up such precise simulations, quantum computing may lead to the development of computational tools that fit into fast-paced laboratory workflows and open up completely new possibilities. In particular, the design-build-test-learn cycle would be better informed in each round, enabling the design of new and better enzyme variants.

Acknowledgements

We thank Amazon Web Services (AWS) for facilitating remote access to IonQ's Aria-1 system and to Rigetti's Aspen-M-3 device through Amazon Braket and supporting this project via the [AWS Cloud Credit for Research](#) program.

References

1. Helgaker, T., Jørgensen, P. & Olsen, J. *Molecular Electronic Structure Theory* (John Wiley & Sons, LTD, Chichester, 2000).
2. Warshel, A. & Karplus, M. Calculation of ground and excited state potential surfaces of conjugated molecules. i. formulation and parametrization. *J. Am. Chem. Soc.* **94**, 5612–5625, DOI: [10.1021/ja00771a014](https://doi.org/10.1021/ja00771a014) (1972).
3. Levitt, M. & Warshel, A. Computer simulation of protein folding. *Nature* **253**, 694–698, DOI: [10.1038/253694a0](https://doi.org/10.1038/253694a0) (1975).

4. Warshel, A. & Levitt, M. Theoretical studies of enzymic reactions: Dielectric, electrostatic and steric stabilization of the carbonium ion in the reaction of lysozyme. *J. Mol. Biol.* **103**, 227–249, DOI: [https://doi.org/10.1016/0022-2836\(76\)90311-9](https://doi.org/10.1016/0022-2836(76)90311-9) (1976).
5. Bharti, K. *et al.* Noisy intermediate-scale quantum algorithms. *Rev. Mod. Phys.* **94**, 015004, DOI: [10.1103/RevModPhys.94.015004](https://doi.org/10.1103/RevModPhys.94.015004) (2022).
6. Ezratty, O. Understanding quantum technologies 2023 (2021). [arXiv:2111.15352](https://arxiv.org/abs/2111.15352).
7. Kim, Y. *et al.* Evidence for the utility of quantum computing before fault tolerance. *Nature* **618**, 500–505, DOI: [10.1038/s41586-023-06096-3](https://doi.org/10.1038/s41586-023-06096-3) (2023).
8. Robledo-Moreno, J. *et al.* Chemistry beyond exact solutions on a quantum-centric supercomputer (2024). [2405.05068](https://arxiv.org/abs/2405.05068).
9. Forster, R. E. *Remarks on the discovery of carbonic anhydrase*, 1–11 (Birkhäuser Basel, Basel, 2000).
10. Tu, C. K. & Silverman, D. N. Mechanism of carbonic anhydrase studied by carbon-13 and oxygen-18 labeling of carbon dioxide. *J. Am. Chem. Soc.* **97**, 5935–5936, DOI: [10.1021/ja00853a060](https://doi.org/10.1021/ja00853a060) (1975). <https://doi.org/10.1021/ja00853a060>.
11. Smedarchina, Z., Siebrand, W., Fernández-Ramos, A. & Cui, Q. Kinetic isotope effects for concerted multiple proton transfer: A direct dynamics study of an active-site model of carbonic anhydrase ii. *J. Am. Chem. Soc.* **125**, 243–251, DOI: [10.1021/ja0210594](https://doi.org/10.1021/ja0210594) (2003). PMID: 12515527, <https://doi.org/10.1021/ja0210594>.
12. Majland, M., Etenhuber, P. & Zinner, N. T. Fermionic adaptive sampling theory for variational quantum eigensolvers. *Phys. Rev. A* **108**, 052422, DOI: [10.1103/PhysRevA.108.052422](https://doi.org/10.1103/PhysRevA.108.052422) (2023).
13. Spicher, S. & Grimme, S. Robust Atomistic Modeling of Materials, Organometallic, and Biochemical Systems. *Angewandte Chemie Int. Ed.* **59**, 15665–15673, DOI: [10.1002/anie.202004239](https://doi.org/10.1002/anie.202004239) (2020).
14. Bannwarth, C. *et al.* Extended tight-binding quantum chemistry methods. *WIREs Comput. Mol. Sci.* **11**, e1493, DOI: <https://doi.org/10.1002/wcms.1493> (2021). <https://wires.onlinelibrary.wiley.com/doi/pdf/10.1002/wcms.1493>.
15. Svensson, M. *et al.* Oniom: A multilayered integrated mo + mm method for geometry optimizations and single point energy predictions. a test for diels-alder reactions and pt(p(t-bu)3)2 + h2 oxidative addition. *The J. Phys. Chem.* **100**, 19357–19363, DOI: [10.1021/jp962071j](https://doi.org/10.1021/jp962071j) (1996). <https://doi.org/10.1021/jp962071j>.
16. Rossmannek, M., Pavošević, F., Rubio, A. & Tavernelli, I. Quantum embedding method for the simulation of strongly correlated systems on quantum computers. *The J. Phys. Chem. Lett.* **14**, 3491–3497, DOI: [10.1021/acs.jpcclett.3c00330](https://doi.org/10.1021/acs.jpcclett.3c00330) (2023). PMID: 37011400, <https://doi.org/10.1021/acs.jpcclett.3c00330>.
17. Izsák, R. *et al.* Quantum computing in pharma: A multilayer embedding approach for near future applications. *J. Comput. Chem.* **44**, 406–421, DOI: <https://doi.org/10.1002/jcc.26958> (2023). <https://onlinelibrary.wiley.com/doi/pdf/10.1002/jcc.26958>.
18. Ma, H. *et al.* Multiscale quantum algorithms for quantum chemistry. *Chem. Sci.* **14**, 3190–3205, DOI: [10.1039/D2SC06875C](https://doi.org/10.1039/D2SC06875C) (2023).
19. Santagati, R. *et al.* Drug design on quantum computers. *Nat. Phys.* **20**, 549–557, DOI: [10.1038/s41567-024-02411-5](https://doi.org/10.1038/s41567-024-02411-5) (2024).
20. Fu, Y., Fan, F., Zhang, Y., Wang, B. & Cao, Z. Conformational change of h64 and substrate transportation: Insight into a full picture of enzymatic hydration of co2 by carbonic anhydrase. *Front. Chem.* **9**, DOI: [10.3389/fchem.2021.706959](https://doi.org/10.3389/fchem.2021.706959) (2021).
21. Jónsson, H., Mills, G. & Jacobsen, K. W. *Nudged elastic band method for finding minimum energy paths of transitions*, chap. Part II The Art of Simulation, 385–404 (World Scientific, 1998). https://www.worldscientific.com/doi/pdf/10.1142/9789812839664_0016.
22. Spicher, S. & Grimme, S. Robust atomistic modeling of materials, organometallic, and biochemical systems. *Angewandte Chemie Int. Ed.* **59**, 15665–15673, DOI: <https://doi.org/10.1002/anie.202004239> (2020). <https://onlinelibrary.wiley.com/doi/pdf/10.1002/anie.202004239>.
23. Bannwarth, C., Ehlert, S. & Grimme, S. Gfn2-xtb—an accurate and broadly parametrized self-consistent tight-binding quantum chemical method with multipole electrostatics and density-dependent dispersion contributions. *J. Chem. Theory Comput.* **15**, 1652–1671, DOI: [10.1021/acs.jctc.8b01176](https://doi.org/10.1021/acs.jctc.8b01176) (2019). PMID: 30741547, <https://doi.org/10.1021/acs.jctc.8b01176>.
24. Ehlert, S., Stahn, M., Spicher, S. & Grimme, S. Robust and Efficient Implicit Solvation Model for Fast Semiempirical Methods. *J. Chem. Theory Comput.* **17**, 4250–4261, DOI: [10.1021/acs.jctc.1c00471](https://doi.org/10.1021/acs.jctc.1c00471) (2021). Publisher: American Chemical Society.

25. Sun, Q. Libcint: An efficient general integral library for gaussian basis functions. *J. Comput. Chem.* **36**, 1664–1671, DOI: <https://doi.org/10.1002/jcc.23981> (2015). <https://onlinelibrary.wiley.com/doi/pdf/10.1002/jcc.23981>.
26. Sun, Q. *et al.* Pyscf: the python-based simulations of chemistry framework. *WIREs Comput. Mol. Sci.* **8**, e1340, DOI: <https://doi.org/10.1002/wcms.1340> (2018). <https://wires.onlinelibrary.wiley.com/doi/pdf/10.1002/wcms.1340>.
27. Sun, Q. *et al.* Recent developments in the PySCF program package. *The J. Chem. Phys.* **153**, 024109, DOI: [10.1063/5.0006074](https://doi.org/10.1063/5.0006074) (2020). https://pubs.aip.org/aip/jcp/article-pdf/doi/10.1063/5.0006074/16722275/024109_1_online.pdf.
28. Manby, F. R., Stella, M., Goodpaster, J. D. & Miller, T. F. I. A simple, exact density-functional-theory embedding scheme. *J. Chem. Theory Comput.* **8**, 2564–2568, DOI: [10.1021/ct300544e](https://doi.org/10.1021/ct300544e) (2012). PMID: 22904692, <https://doi.org/10.1021/ct300544e>.
29. Rubin, N. C. A hybrid classical/quantum approach for large-scale studies of quantum systems with density matrix embedding theory (2016). [1610.06910](https://arxiv.org/abs/1610.06910).
30. Li, W. *et al.* Toward practical quantum embedding simulation of realistic chemical systems on near-term quantum computers. *Chem. Sci.* **13**, 8953–8962, DOI: [10.1039/D2SC01492K](https://doi.org/10.1039/D2SC01492K) (2022).
31. Vorwerk, C., Sheng, N., Govoni, M., Huang, B. & Galli, G. Quantum embedding theories to simulate condensed systems on quantum computers. *Nat. Comput. Sci.* **2**, 424–432, DOI: [10.1038/s43588-022-00279-0](https://doi.org/10.1038/s43588-022-00279-0) (2022).
32. Grimsley, H. R., Economou, S. E., Barnes, E. & Mayhall, N. J. An adaptive variational algorithm for exact molecular simulations on a quantum computer. *Nat. Commun.* **10**, 3007, DOI: [10.1038/s41467-019-10988-2](https://doi.org/10.1038/s41467-019-10988-2) (2019). Number: 1 Publisher: Nature Publishing Group.
33. Knizia, G. Intrinsic atomic orbitals: An unbiased bridge between quantum theory and chemical concepts. *J. Chem. Theory Comput.* **9**, 4834–4843, DOI: [10.1021/ct400687b](https://doi.org/10.1021/ct400687b) (2013). PMID: 26583402, <https://doi.org/10.1021/ct400687b>.
34. Sosa, C., Geertsen, J., Trucks, G. W., Bartlett, R. J. & Franz, J. A. Selection of the reduced virtual space for correlated calculations. an application to the energy and dipole moment of h2o. *Chem. Phys. Lett.* **159**, 148–154, DOI: [https://doi.org/10.1016/0009-2614\(89\)87399-3](https://doi.org/10.1016/0009-2614(89)87399-3) (1989).
35. Jordan, P. & Wigner, E. Über das paulische äquivalenzverbot. *Zeitschrift für Physik* **47**, 631–651, DOI: [10.1007/BF01331938](https://doi.org/10.1007/BF01331938) (1928).
36. Yordanov, Y. S., Armaos, V., Barnes, C. H. W. & Arvidsson-Shukur, D. R. M. Qubit-excitation-based adaptive variational quantum eigensolver. *Commun. Phys.* **4**, 228, DOI: [10.1038/s42005-021-00730-0](https://doi.org/10.1038/s42005-021-00730-0) (2021).
37. Jensen, F. Unifying general and segmented contracted basis sets. segmented polarization consistent basis sets. *J. Chem. Theory Comput.* **10**, 1074–1085, DOI: [10.1021/ct401026a](https://doi.org/10.1021/ct401026a) (2014). <https://doi.org/10.1021/ct401026a>.
38. Shaik, I. & van de Pol, J. Optimal layout-aware cnot circuit synthesis with qubit permutation. In *ECAI'24* (IOS Press, Santiago de Compostela, Spain, 2024).
39. Sivarajah, S. *et al.* tl ket>: a retargetable compiler for nisq devices. *Quantum Sci. Technol.* **6**, 014003 (2020).
40. Kanno, K. *et al.* Quantum-selected configuration interaction: classical diagonalization of hamiltonians in subspaces selected by quantum computers (2023). [2302.11320](https://arxiv.org/abs/2302.11320).
41. Nakagawa, Y. O., Kamoshita, M., Mizukami, W., Sudo, S. & ya Ohnishi, Y. Adapt-qsci: Adaptive construction of input state for quantum-selected configuration interaction (2023). [2311.01105](https://arxiv.org/abs/2311.01105).
42. von Burg, V. *et al.* Quantum computing enhanced computational catalysis. *Phys. Rev. Res.* **3**, 033055, DOI: [10.1103/PhysRevResearch.3.033055](https://doi.org/10.1103/PhysRevResearch.3.033055) (2021).

A Orbital assignment

After some investigation, we finally opted for a simple ranking strategy for selecting the orbitals to be included in the fragment A which is defined as a collection of atomic indices. Such a strategy may be constructed by ranking occupied local orbitals according to the simple weight defined as

$$w_i = \sum_{a \in A} \sum_{\mu \in \mathcal{B}_a} |C_{\mu i}|, \quad (6)$$

where i refers to the specific localized (occupied) orbital, a is the index for an atom included in subsystem A , \mathcal{B}_a is the list of atomic orbital indices associated with atom a , and $C_{\mu i}$ is the coefficient for the μ -th atomic orbital contributing to the specific localized orbital i . The set $\{w_i\}$ is computed at each point along the reaction coordinate and a fixed number of orbitals is assigned to region A at each point. The number of orbitals in region A is somewhat arbitrary and we have therefore chosen to determine a number n at the transition state structure based on

$$f(i) = \arg \max_{a \in A \cup B} \sum_{\mu \in \mathcal{B}_a} |C_{\mu i}|, \quad (7)$$

$$n = \sum_{b \in A} \sum_i \delta_{b, f(i)}. \quad (8)$$

Here $f(i)$ is a function that maps an orbital i to the atom a at which i has the largest cumulative weight and n then counts the number of orbitals assigned to any atoms in A .

B MP2 based FNO construction

In the occupied subspace of fragment A and all virtual orbitals another HF calculation is required before executing the correlation energy calculation on a quantum device. Instead of directly constructing the subspace Hamiltonian from the HF calculation, we perform an MP2 calculation afterwards using the same number of occupied orbitals as the number of electrons specified in the active space, starting from the Fermi level. We then use the resulting MP2 amplitudes t_{ij}^{ab} to construct the virtual correlation density matrix defined in Eq.(9)

$$d_{ab} = \sum_{c, j} t_{ij}^{ac} t_{ij}^{cb} \quad (9)$$

which may be diagonalized to define a new set of (natural) virtual orbitals which are then included according to the absolute size of the corresponding eigenvalue, starting with the largest values until the desired amount of orbitals is obtained. While not perfect, the selected correlation spaces are reasonable due to both a locality and energy/eigenvalue selection criterion and can capture some static and dynamic electronic correlation.

The actual size of the active space is defined by the number of qubits available, thus by the hardware, and for the present calculations we have used 6 electrons in 6 spatial orbitals corresponding to 12 qubits (one for each spin-orbital).

C Corrected singles and doubles circuits

Here we present the corrected singles and doubles excitation operators from Yordanov *et al*³⁶ as implemented in our software.

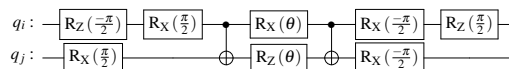


Figure 7. Corrected parametrized singles excitations circuit

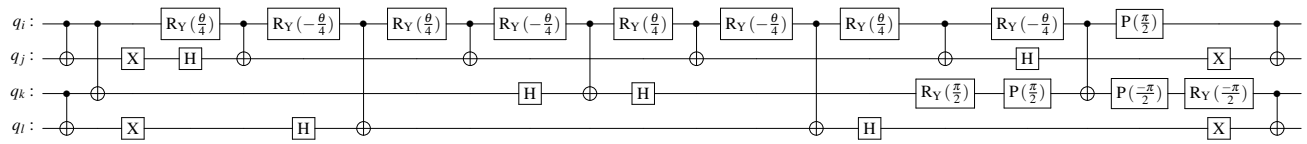


Figure 8. Corrected parametrized double excitation circuit.